Hindawi Publishing Corporation
Applied and Environmental Soil Science
Volume 2016, Article ID 1480976, 15 pages
http://dx.doi.org/10.1155/2016/1480976

Research Article

Combining Geoelectrical Measurements and CO_2 Analyses to Monitor the Enhanced Bioremediation of Hydrocarbon-Contaminated Soils: A Field Implementation

Cécile Noel,[1,2] Jean-Christophe Gourry,[1] Jacques Deparis,[1] Michaela Blessing,[1] Ioannis Ignatiadis,[1] and Christophe Guimbaud[2]

[1]*BRGM, 3 avenue Claude Guillemin, 45060 Orléans, France*
[2]*LPC2E, CNRS, 3 avenue de la Recherche Scientifique, 45071 Orléans, France*

Correspondence should be addressed to Cécile Noel; cecile.noel@cnrs-orleans.fr

Received 2 October 2015; Accepted 12 November 2015

Academic Editor: Pantelis Soupios

Hydrocarbon-contaminated aquifers can be successfully remediated through enhanced biodegradation. However, *in situ* monitoring of the treatment by piezometers is expensive and invasive and might be insufficient as the information provided is restricted to vertical profiles at discrete locations. An alternative method was tested in order to improve the robustness of the monitoring. Geophysical methods, electrical resistivity (ER) and induced polarization (IP), were combined with gas analyses, CO_2 concentration, and its carbon isotopic ratio, to develop a less invasive methodology for monitoring enhanced biodegradation of hydrocarbons. The field implementation of this monitoring methodology, which lasted from February 2014 until June 2015, was carried out at a BTEX-polluted site under aerobic biotreatment. Geophysical monitoring shows a more conductive and chargeable area which corresponds to the contaminated zone. In this area, high CO_2 emissions have been measured with an isotopic signature demonstrating that the main source of CO_2 on this site is the biodegradation of hydrocarbon fuels. Besides, the evolution of geochemical and geophysical data over a year seems to show the seasonal variation of bacterial activity. Combining geophysics with gas analyses is thus promising to provide a new methodology for *in situ* monitoring.

1. Introduction

Petroleum hydrocarbon leaks and accidental spills happen commonly during the production, refining, transport, and storage of petroleum. Release of petroleum hydrocarbons into the environment causes damage to ecosystems [1] and to soil and water resources [2]. Increasing demand for drinking water and cropland with population growth requires effective remediation techniques to treat the contamination and to decrease hostile effects on health and environment. *In situ* remediation techniques such as enhanced bioremediation were shown to be effective in cleanup of the contamination [3, 4]. Enhanced bioremediation involves the addition of nutrients or electron acceptors to the subsurface environment to accelerate the natural biodegradation processes which degrade hydrocarbons [5]. Due to the potential of cost saving of *in situ* techniques compared to conventional *ex situ* techniques, there is an economical interest for commercial providers to use enhanced bioremediation [6]. However, these processes remain partially unexploited, mainly because their *in situ* monitoring, before, during, and after soil treatment operations, is often expensive and technically challenging. Indeed, where significant subsurface heterogeneity exists, conventional intrusive groundwater sampling campaigns can be insufficient to obtain relevant information as they are restricted to costly monitoring piezometers at discrete locations. New monitoring tools are needed to overcome these limitations and make the enhanced bioremediation more reliable and robust, as well as economically competitive.

Previous studies suggest that geoelectrical techniques, especially electrical resistivity (ER) and induced polarization (IP), can be used to detect the presence of LNAPLs (Light Nonaqueous Phase Liquids) [7–10] as well as monitoring the effects of their biodegradation [11–14]. Biodegradation

processes modify ground electrical properties because they change biophysicochemical conditions in the subsurface: (i) bacteria modify local redox conditions, inducing changes in self-potential (SP) [15]; (ii) microbial activity can produce organic acids and/or carbonic acid that affect the pore water conductivity, modifying both the in-phase and the quadrature conductivity [16]; (iii) during microbial growth and formation of biofilms, biomass can clog pores and potentially change the porosity and hydraulic conductivity, increasing the storage of electrical charges [17, 18]. Thus, ER and IP are expected to be effective nonintrusive tools to monitor enhanced bioremediation.

Some studies have implemented geoelectrical methods to characterize hydrocarbon-contaminated sites under biodegradation [19–22], but only few apply these methods for long-term monitoring or to prove the efficiency of enhanced bioremediation [23]. These previous field studies suggest that ER and IP are highly sensitive to the biophysicochemical processes associated with biodegradation. Nevertheless, the interpretation of geophysical data remains challenging partly because several factors may contribute to the observed electrical response (presence of metallic particles or clays, e.g.) and/or influence the electrical response in function of time (variation of water saturation and temperature). That is why geoelectrical methods are often used in conjunction with geochemical measurements (temperature, pH, redox potential, water conductivity, and dissolved oxygen content) to detect changes in the chemical and physical properties of the soil and groundwater. With the aim of minimizing the use of piezometers, microbial activity is followed by studying gas emissions at the ground surface. Indeed, aerobic degradation of hydrocarbons results in the production of CO_2 [24]. Due to its limited solubility (in alkalinity saturated groundwaters), CO_2 gas will tend to migrate toward the ground surface and surface CO_2 fluxes can be directly linked to the biodegradation intensity. Meanwhile, this CO_2 production occurs concurrently with natural root and microbial soil respiration. Thus, tools capable of quantifying CO_2 sources are also needed. Carbon stable isotopic analyses (ratio of $^{13}C/^{12}C$) use the fact that petroleum hydrocarbon isotopic signature is distinguishable (range from −18 to −34‰ versus Vienna Pee Dee Belemnite or VPDB [25]) from other aquifer components: for example, carbonate minerals have a signature between +2 and −12‰ versus VPDB [26] and the C_3 plants (plants that use the Calvin or C_3 cycle of carbon fixation) produce organic matter with isotopic signature near −25 ± 5‰ versus VPDB [25, 27, 28]. Moreover, bacteria can induce a carbon isotopic fractionation as they preferentially use the lighter isotope ^{12}C (due to the lower energy required to break intramolecular bonds) [29]. Some studies linked the CO_2 production with contaminant degradation rate in laboratory [30–32] and at contaminated field sites [33]. Some researchers have examined the isotopic signature of CO_2 and dissolved inorganic carbon from aerobic biodegradation of petroleum hydrocarbons to support their analysis [34–38]. Results reflect the difficulty in definitively attributing CO_2 produced from biodegradation of contaminants versus that from possible interferences of background CO_2 under field conditions. The other natural sources of CO_2, plant root respiration in shallow sediments and carbonate dissolution in subsurface sediments, must be taken into account in field experiments [25].

Integrating both geoelectrical methods and gas analyses could help to develop a less invasive technique with a little geochemical sampling in piezometers in order to monitor enhanced biodegradation of hydrocarbons. These tools were previously tested at laboratory scale in sand-columns with toluene as model pollutant and an exogenous bacterial strain [39]. The promising results from the column study allowed implementing a monitoring strategy at the field scale. The site was a gasoline station where gasoline and diesel fuels leaked eighteen years ago. A reactive barrier supplied the necessary oxygen to the aquifer in order to stimulate the aerobic bacterial processes since April 2014. Geoelectrical measurements and ER and IP surveys, as well as CO_2 analyses, had been performed from February 2014 until June 2015 on this site.

2. Materials and Methods

The experimentation had been implemented at a gasoline station over a 16-month period, from February 2014 to June 2015. After a preliminary characterization of the site (baseline, February 2014), and the start of the oxidative reactive barrier in April 2014, the long-term monitoring had been carried out.

The site had been equipped to monitor time-lapse changes in electrical properties of the subsurface with electrical resistivity (ER) and time domain induced polarisation (TDIP) systematic 2D tomographies. This monitoring had been combined with regular CO_2 fluxes measurements and its carbon isotopic ratio at the ground surface.

The indirect monitoring was completed with several analyses in piezometers to assess the nonintrusive survey: (i) measurements of pollutant concentration and carbon isotopic signature of selected aromatic hydrocarbons and (ii) monitoring of groundwater physicochemical properties with probes.

2.1. Site Description. The site studied was a gasoline station where gasoline and diesel fuels leaked in 1997 (Figure 1). It is still in activity but the former tank installation (source of contamination) was dismantled. Several piezometers had been drilled for previous studies on this site. These studies showed that

(i) the ground was mainly composed of silts and clays: a first layer (thickness ranging from 0.5 to 3.5 m) of backfills made of brown silts, which often contained gravels, followed by a succession of loamy strata, with varying degrees of sands, and even sandy clays with limestone or millstone blocks (until 5 to 7.5 m depth); and then argillaceous limestones are interbedded with thin layers of sandy clays;

(ii) the ground had a low permeability (between 10^{-6} and 10^{-7} m/s);

(iii) the direction of flow was northwest;

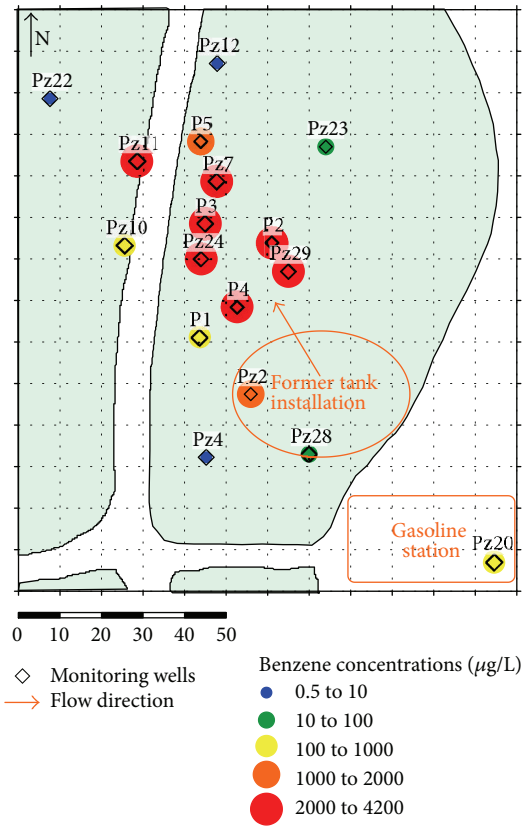

Figure 1: Map of the site showing gasoline station, former tank installation, monitoring piezometers, and the benzene concentrations measured in water in September 2013.

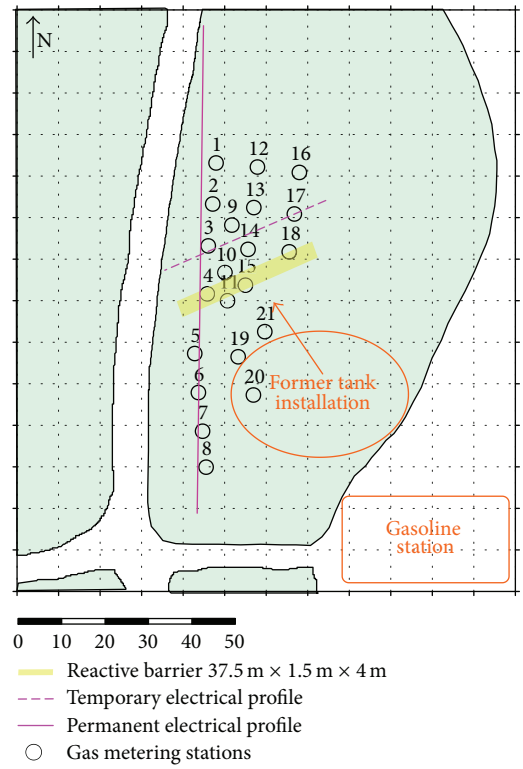

Figure 2: Map of the site showing the reactive barrier and the monitoring disposal: 2 electrical profiles and 21 gas metering stations.

(iv) the water table depth ranged between 2.5 and 4.5 m and depends on seasons (winter, summer);

(v) there was a presence of hydrocarbons in the area of the former tank installation and the fraction of benzene, toluene, ethylbenzene, and xylenes (BTEX) represented a consequent part of the pollutants (Figure 1);

(vi) there were indications of a natural attenuation (hydrocarbon degradation) which prove the presence of a bacterial flora, such as absence of dissolved oxygen, that matched the BTEX plume in water [40].

An important limiting factor in bioremediation of soils contaminated with hydrocarbons is the lack of oxygen to support microbial activities [41, 42]. Injection of aqueous H_2O_2 was the selected method to overcome this limitation and to stimulate aerobic metabolic processes.

A permeable reactive barrier of 4 m depth × 35 m long × 1.5 m wide was implemented to stop the plume migration (Figure 2). The site was equipped with 3 pumping wells just upstream the barrier, 3 injection wells in the barrier, and 2 injection wells just downstream the barrier. Pumped water was filtered through active charcoal. After filtration, diluted H_2O_2 was added to the treated water and oxygenated water was reinjected in the barrier, through the 3 injection wells, slotted from −2 to −4 m in order to deliver oxygen in the upper part of the water table. The permeability of this barrier (10^{-3} m/s) allowed an homogeneous distribution of the treating fluid. Finally, the last part of the oxygenated water was injected in 2 boreholes downstream the barrier, slotted from −6 to −8 m, to bring oxygen in the deepest part of the water table. The biostimulation was started in April 2014.

2.2. Electrical Geophysical Measurements. Geophysical methods are a standard tool for obtaining information on volumetric distributions of subsurface physical properties of rocks and fluids. Among several electrical methods which measure electrical properties of the ground, two of them were used: the electrical resistivity (ER) and the time domain induced polarization (TDIP).

In a typical ER measurement, four electrodes are used. ER instrumentation measures potential differences between pairs of electrodes, where the potentials result from a current applied by the instrumentation between two other electrodes. By making measurements with current and potential electrodes at many different locations, one can collect sufficient data which allow the construction of an electrical resistivity section (a 2D slice of the earth).

Whereas ER is sensitive to pore fluid resistivity (and consequently to total dissolved solids or ionic strength), the IP method measures the capacitive behaviour of the subsurface, which strongly depends on the properties of the mineral surface. Different studies have shown the sensitivity of IP to mineral precipitation and changes occurring at

pore-grain interfaces, where biological reactions occur [12]. TDIP measurements use the same instrumentation as ER measurements. Here, the injected current is alternately ON and OFF. The decrease of the induced voltage is measured to calculate the chargeability, which is the ground capacity to store charges. Hereafter, in this paper, the normalized chargeability (defined as the chargeability divided by the resistivity magnitude) will be calculated to free the chargeability from variation of resistivity [43].

Two time domain ER and IP profiles were carried out at the study site. Positioning of the profiles was performed according to the contaminant plume and barrier location: both profiles went across the plume, one was perpendicular to the barrier, and the other was parallel, 8 m downstream the barrier (Figure 2).

The perpendicular profile was buried permanently at 50 cm of depth. Apparent resistivity and chargeability measurements were obtained using a system with 60 stainless steel electrodes: 30 electrodes, with a constant spacing of 4 m, were dedicated to current injection, and the other 30, with a spacing of 4 m as well, were used for potential measurement to avoid electromagnetic (EM) coupling effect. The two sets of electrodes are disposed staggered, so that each electrode is laid out at a constant interval of 2 m. To achieve a good lateral resolution and to avoid EM coupling effect, the dipole-dipole array was applied to obtain the apparent resistivity and chargeability pseudosections. A Syscal R1+ (from IRIS Instruments©, Orleans, France) has been used in this study. Measurements were performed continuously every two days. The second profile, parallel to the barrier, was a temporary profile. It consists in 48 electrodes separated by 1 m. Measurements were performed every two months with an Elrec Pro (IRIS Instruments, Orleans, France).

After performing time-lapse ER and IP measurements, the electrical data were analysed in three stages:

(i) Initial anomalous data were filtered by a process of elimination:
   (a) current $I < 100$ mA;
   (b) potential $V < 0.1$ mV;
   (c) apparent chargeability $m < 0$;
   (d) error $Q > 5\%$ (resistivity measurements) and $Q > 2\%$ (chargeability measurements);

(ii) The quadrupoles in common to all the data sets were selected;

(iii) Data processing was performed with RES2DINV software [44], in time-lapse mode. The process is based on several iterations comparing the measured data with a model calculated by the software for each time series data set. This process enables obtaining a 2D distribution of resistivity and chargeability sections at every time. The following settings were used to define the type of constrains applied during the time-lapse inversion process:
   (a) The relative importance given to minimize the difference between models at different times is controlled by the time-lapse damping factor. A value of 0 to 5 can be generally used: if a value of 0 is used, the inversion of the different time series data sets would be carried out independently; if a value of 1 is used, equal weight would be given to reducing the difference between the models at different times; a larger value of the damping factor forces the different time models to be more similar. After some previous tests, a value of 3 was selected.
   (b) Time-difference roughness filter was set for "smooth changes" between time models.
   (c) The maximum number of iterations was 5.

2.3. CO_2 Analyses: Emissions Fluxes and Carbon Isotopic Ratio. The geoelectrical measurements were combined with CO_2 analyses. The measurements of CO_2 effluxes at the ground surface demonstrate the occurrence and rate of aerobic hydrocarbon biodegradation [33]. However, to determine the accuracy of the method, contaminated-derived soil respiration must be distinguished from chemistry of mineral-carbonates and from the natural soil respiration, resulting from biodegradation of dead organic matter and plant root respiration.

CO_2 produced by fossil hydrocarbon degradation may be distinguished from that produced by other processes based on the carbon isotopic compositions, characteristic of the source material, and/or fractionation accompanying microbial metabolism. Indeed, carbon isotopic signature of CO_2 reaches those of contaminant and it can be accompanied by significant carbon isotope fractionation [37].

Stable isotopic ratio represents the abundance of the rare isotope with respect to the abundant isotope ($^{13}C/^{12}C$). Due to slight analytical variations, it is common to compare isotopic ratios measured in an unknown sample to those in a standard material; this results in the delta notation:

$$\delta^{13}\mathrm{C}\,(‰) = \left[\frac{\left(^{13}\mathrm{C}/^{12}\mathrm{C}\right)_{\mathrm{sample}}}{\left(^{13}\mathrm{C}/^{12}\mathrm{C}\right)_{\mathrm{VPDB}}} - 1\right] * 1000 \qquad (1)$$

with $(^{13}C/^{12}C)_{VPDB} = 0.011237$ [45].

CO_2 concentration and $\delta^{13}C$ isotopic ratio in produced CO_2 are measured by a high-resolution laser infrared spectrometer, called SPIRIT (Spectrometer Infrared *In Situ* Tropospheric) and developed by the LPC2E (CNRS, Orleans, France). This spectrometer is an adaptation of the original SPIRIT, described in Guimbaud et al. (2011) [46] and used for greenhouse gas emissions at the air-land interface [47, 48], by the implementation of a quantum cascade laser using the $^{12}CO_2$ and $^{13}CO_2$ ro-vibrational lines. The uncertainty for $\delta^{13}C$ determination on field deployment is on the order of 0.4‰. A complete description of the adapted SPIRIT for $^{13}C/^{12}C$ isotopic ratio quantification is available in Guimbaud et al. [49]. The spectrometer is directly connected with a closed accumulation chamber set on a permanent PVC cylinder collar (diameter = 30 cm) sunk into the soil to measure CO_2 emission fluxes and $\delta^{13}(CO_2)$. The ground

Table 1: List of probes in the monitoring piezometers (function and depth).

Monitoring piezometer	Probes	Depth (m)
Pz4	O_2	6.15
	Water level	4.15
	Conductivity	4
Pz7	O_2	3.68
	Conductivity	4.13
Pz2	Temperature A	5.29
	Temperature B	7.36
	Temperature C	9.3
	Water level	6.3
P2	Temperature	5.09
Pz24	O_2	4.98
	Conductivity	5.14
P4	O_2	5.09
	Conductivity	4.98
	Water level	5.06

surface inside the PVC collar was cleared of vegetation (grass, roots) over 15 cm depth. We had 21 measuring points on the site, upstream, above, and downstream the reactive barrier (Figure 2). Measurements were performed every two months since February 2014.

2.4. Geochemical Monitoring in Piezometers. To assess the indirect monitoring of the enhanced bioremediation, chemical analyses were performed every two months in water samples from monitoring piezometers. BTEX concentration and carbon isotopic ratios of these BTEX were measured. Moreover, some piezometer probes had measured continuously the water table level, temperature, conductivity, and oxygen rate in monitoring piezometers (Table 1).

3. Results

3.1. Baseline Characterization. Baseline characterization consisted of collecting datasets prior to the oxygen injection (February-March 2014).

3.1.1. Geophysical Data. Figure 3 shows the results for the permanent profile in March 2014. This profile went through the barrier (metric point 51 m) and was within close proximity to several piezometers (from north to south: Pz12, P5, Pz7, P3, Pz24, P1, and Pz4) whose positions are plotted on Figure 3. The temporary profile was located around 8 m downstream the barrier and it overlapped with two piezometers (from west to east: Pz24 and P2, Figure 4).

The electrical resistivity tomography from the permanent profile showed resistivities between 40 and 80 Ω·m, over the 6 first meters, which correspond to the sandy-loamy layer of the aquifer. From 6-meter depth, resistivity was much smaller (<20 Ω·m) and this may be associated with a sandy clay level. The tomography from the temporary profile displayed the same resistivity range since the pilot site is quite homogeneous. Nevertheless, areas less resistant (<30 Ω·m)

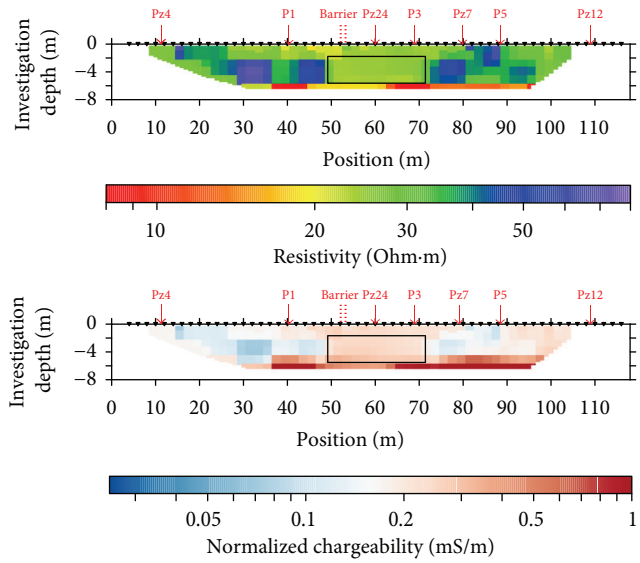

Figure 3: Resistivity and normalized chargeability sections across the plume for the permanent electrical profile, on 6th March 2014. The black rectangle highlights a zone of lower resistivity and higher normalized chargeability.

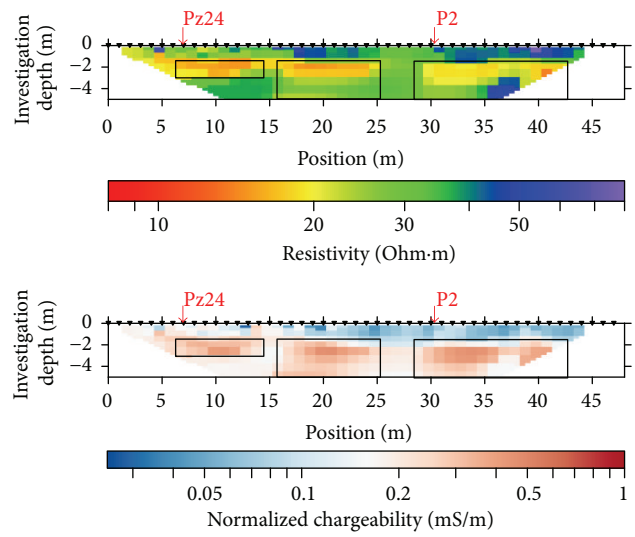

Figure 4: Resistivity and normalized chargeability sections across the plume for the temporary electrical profile, on 6th March 2014. The black rectangles highlight zones of lower resistivity and higher normalized chargeability.

could be identified between 1.5 and 6 m depth, on both profiles:

(i) Between the metric points 50 and 72 m for the permanent profile.

(ii) Between the metric points 7 and 14 m; 16 and 25 m; and 29 and 42 m, for the temporary profile.

Regarding the normalized chargeability tomographies (chargeability divided by resistivity), the values were in the range of 0.025 to 1 mS/m, and the zones of higher normalized

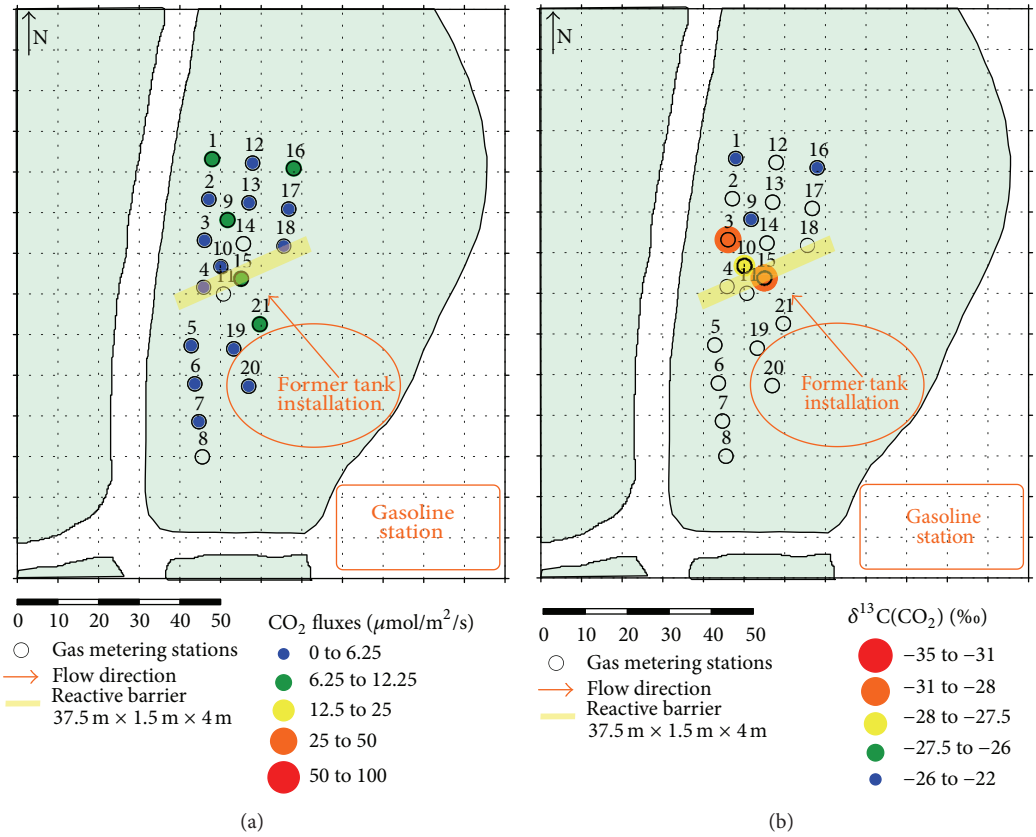

Figure 5: Maps of measured CO_2 emissions (a) and its carbon isotopic ratio versus VPDB (b), in February 2014.

chargeability (>0.2 mS/m) matched the lower resistivity zones. These normalized chargeability anomalies correspond to a polarization effect. On the permanent profile, the normalized chargeability was quite high beyond 6 m depth. This confirms the presence of clays, very chargeable, at these depths.

According to the geochemical data (Figure 1), the localization of these anomalies (higher normalized chargeability and lower resistivity) matched the hydrocarbon polluted area, downstream the former tank installation, at the top of the water table, where natural biodegradation produces conductive byproducts and where chargeable bacteria are numerous (proximity of an organic carbon source).

3.1.2. SPIRIT Data. Figure 5 displays the maps of measured CO_2 emissions and its carbon isotopic ratio in February 2014. There were quite high CO_2 emissions on this site, around 3.8 μmol·m^{-2}·s^{-1}, despite the fact that, during cold periods (December–March), gas fluxes are presumably very low [50, 51]. These results were consistent with those found by Sihota et al. (2011) [33] where the average CO_2 efflux associated with contaminant degradation in the hydrocarbon-contaminated zone was estimated at 2.6 μmol·m^{-2}·s^{-1}. Moreover, the measured $\delta^{13}C(CO_2)$, ranging between −22.2 ± 0.4‰ and −28.8 ± 0.4‰ versus VPDB (averaging −25.3 ± 3‰), were very negative compared to $\delta^{13}C$ of atmospheric CO_2 (around −11‰ versus VPDB, one meter above the ground) and distinguishable from $\delta^{13}C$ of CO_2 from vegetation respiration (around −28‰ versus VPDB [25, 27, 28]). This was an indication of natural biodegradation of hydrocarbons. Indeed, during biodegradation, CO_2 has an isotopic signature near those of the carbon source, which is quite negative in the case of fossil organic carbon (range from −23 to −29‰ versus VPDB for the BTEX of the site [40]).

3.2. Cleanup Progress after One Year of Biostimulation. Figure 6 presents the BTEX (benzene, toluene, ethylbenzene, and xylenes) concentrations over time for 4 piezometers, between February 2014 (two months before barrier activation) and April 2015 (one year after barrier activation). There was an increase in the pollutant concentrations due to the remobilization of contaminants during the barrier construction. The discharge of BTEX may have had significantly slowed down the oxygen diffusion downstream the barrier: it had been quickly consumed and the amount of H_2O_2 could not be increased for avoiding bacteria stress. And, one year after the beginning of biostimulation, there was just a little decrease in benzene and toluene concentrations.

3.3. One Year of Electrical Monitoring. Before barrier activation, it was possible to localize a zone of natural biodegradation on the permanent and the temporary profile (Figures 3 and 4). Figure 7 shows the evolution of the electrical data over a year of enhanced biodegradation, for the permanent profile.

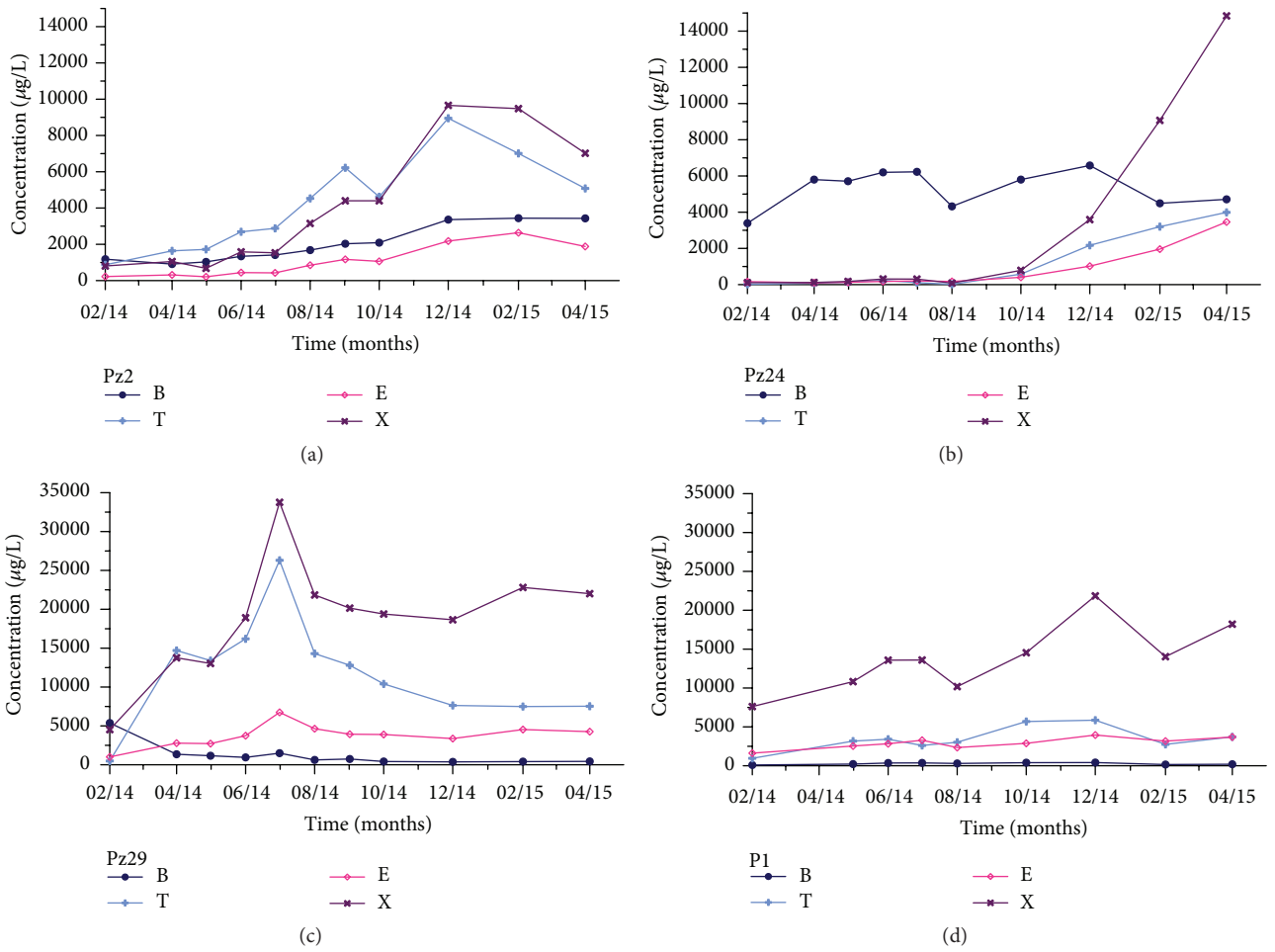

FIGURE 6: Evolution of BTEX (benzene, toluene, ethylbenzene, and xylenes) concentrations in water over time, measured in four monitoring piezometers: Pz2 (a), Pz24 (b), Pz29 (c), and P1 (d), between February 2014 and April 2015.

The resistivity model sections were obtained after time-lapse inversion of 12 datasets, spaced about a month, acquired between March 2014 and April 2015. The convergence of iterative inversion is excellent (<1% for resistivity and <2 for normalized chargeability) and it is comparable with the noise level of the resistivity meter (1%, according to Iris Instruments).

In order to compare the electrical data taking into account the impact of temperature and water saturation on electrical resistivity and chargeability, the inversed data were considered only in the saturated zone and adjusted at 25°C thanks to a linear law [52, 53]:

$$\frac{\rho_{25}}{\rho_T} = \alpha * (T - 25) + 1, \quad (2)$$

where ρ_T is resistivity at temperature T (°C), ρ_{25} is resistivity at 25°C, and α (°C^{-1}) is a temperature compensation factor. The temperature compensation factor α was calculated based on Pz4 (located in a nonpolluted area) temperature data and found to be equal to 0.014, which means that resistivity decreases by 1.4% when temperature increases by 1°C.

Figure 7 shows the anomaly of lower resistivity and higher normalized chargeability on all the tomographies, from March 2014 to April 2015. It was possible to identify two periods of decreasing resistivity and increasing normalized chargeability: a first period from March 2014 to October 2014, and a second period from March 2015 to April 2015. In order to quantify the evolution of the differences, the percentage difference of resistivity and normalized chargeability from March 2014 were calculated (Figure 8). A decrease in resistivity up to 15% is noticed in the area of interest (between metric points 50 and 70 m) at the end of the summer of 2014. However, such a seasonal variation cannot be seen on water conductivity (Figure 9(a)). Regarding normalized chargeability, the tendency is less clear and there are increases outside the area of interest as well.

3.4. One Year of CO_2 (Fluxes and Carbon Isotope Ratio) Monitoring. Gas monitoring was carried out every one-two months, between February 2014 and June 2015. The time allowed for measurements was very short (2 days per campaign). As a consequence, priority was given to flux measurements and then to isotopic ratio measurements of metering points with the highest emissions (more accurate).

CO_2 fluxes ranged between 2.5 and 100 μmol·m^{-2}·s^{-1} (Figure 10(a)). As there was no vegetation inside the PVC

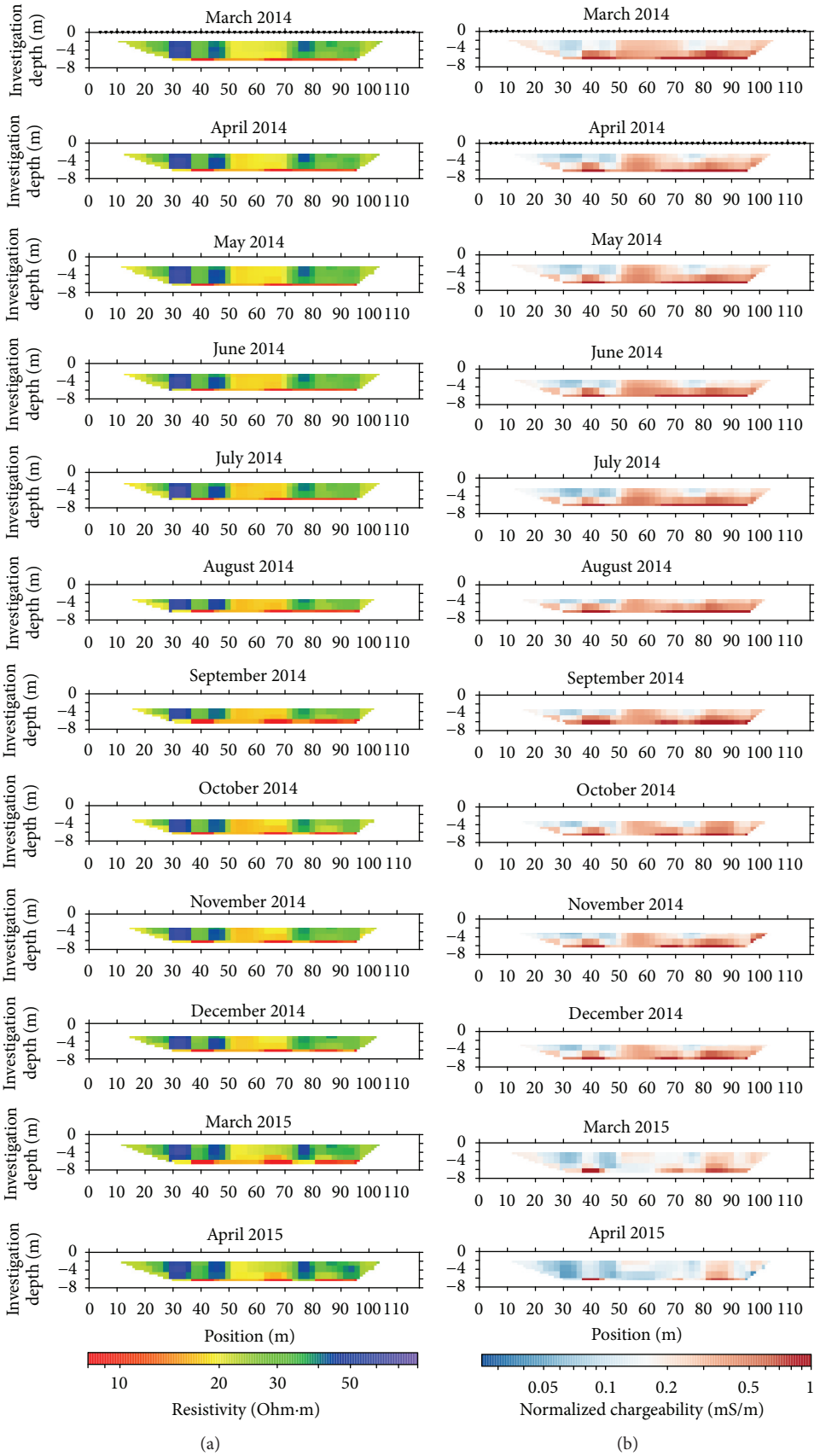

Figure 7: Resistivity (a) and normalized chargeability (b) sections, adjusted at 25°C in the saturated zone, for the permanent electrical profile, between March 2014 and April 2015. The inversion results were obtained after 5 iterations, with 0.58 and 1.82% of error for resistivity and chargeability, respectively.

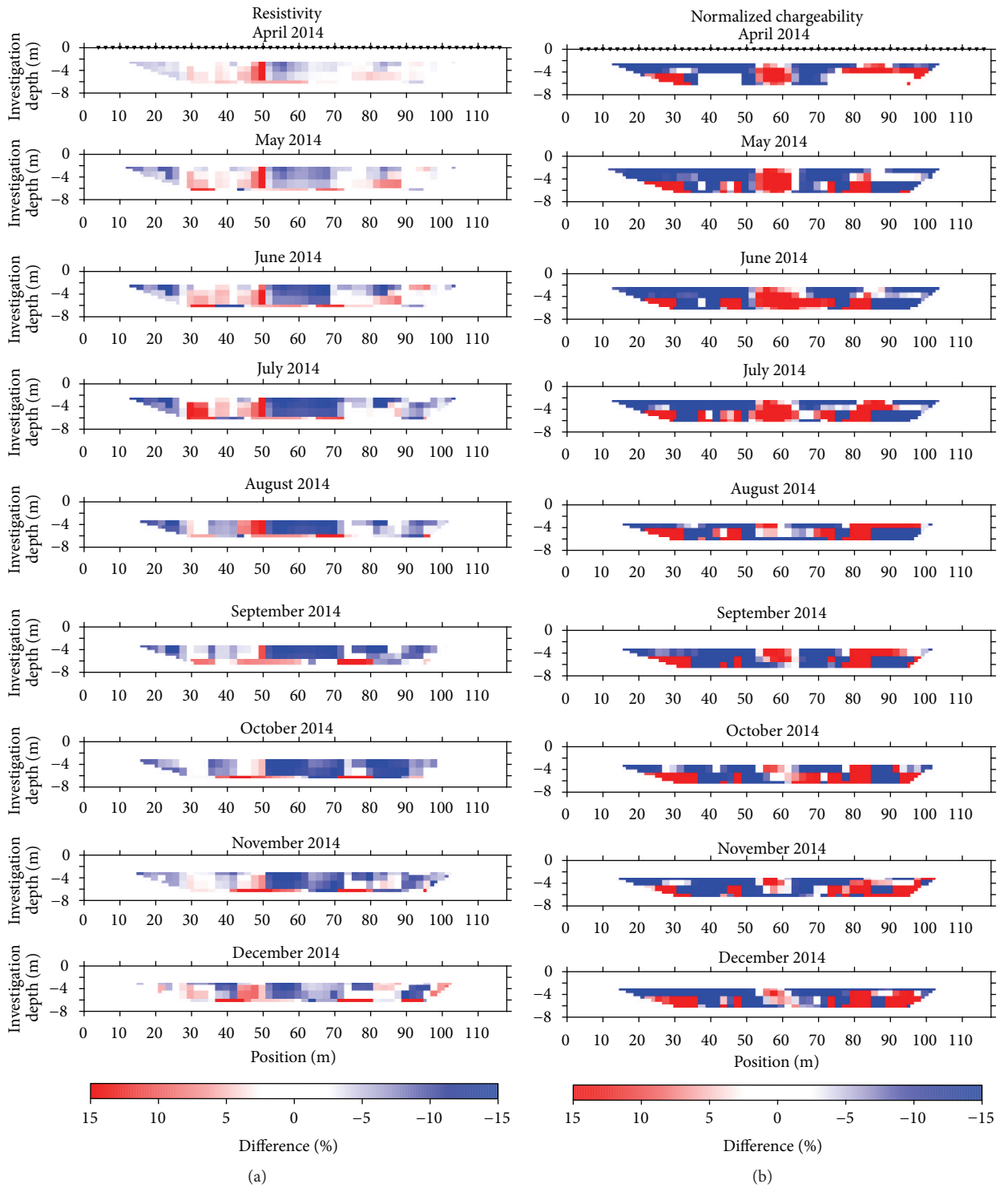

FIGURE 8: Percentage difference (P) over March 2014 of resistivity ρ (a) and normalized chargeability nm (b) sections, for the permanent electrical profile, with $P_\rho = (\rho_{ti} - \rho_{t0})/\rho_{t0} * 100$ and $P_{nm} = (nm_{ti} - nm_{t0})/nm_{t0} * 100$.

collar used to put the SPIRIT chamber, the CO_2 released at the ground surface should come from degradation of soil organic matter and mainly from hydrocarbon biodegradation. The lower emissions were recorded in February 2014. Then, they gradually increased up to August 2014, and decreased during winter 2014-2015. However, meteorological conditions affect gas emissions: CO_2 fluxes were lower when temperatures were low and ground was wet (high rainfalls) (Figure 10) [50]. In order to throw off this effect, we chose a reference measuring point, no. 7, located in the nonpolluted area, where

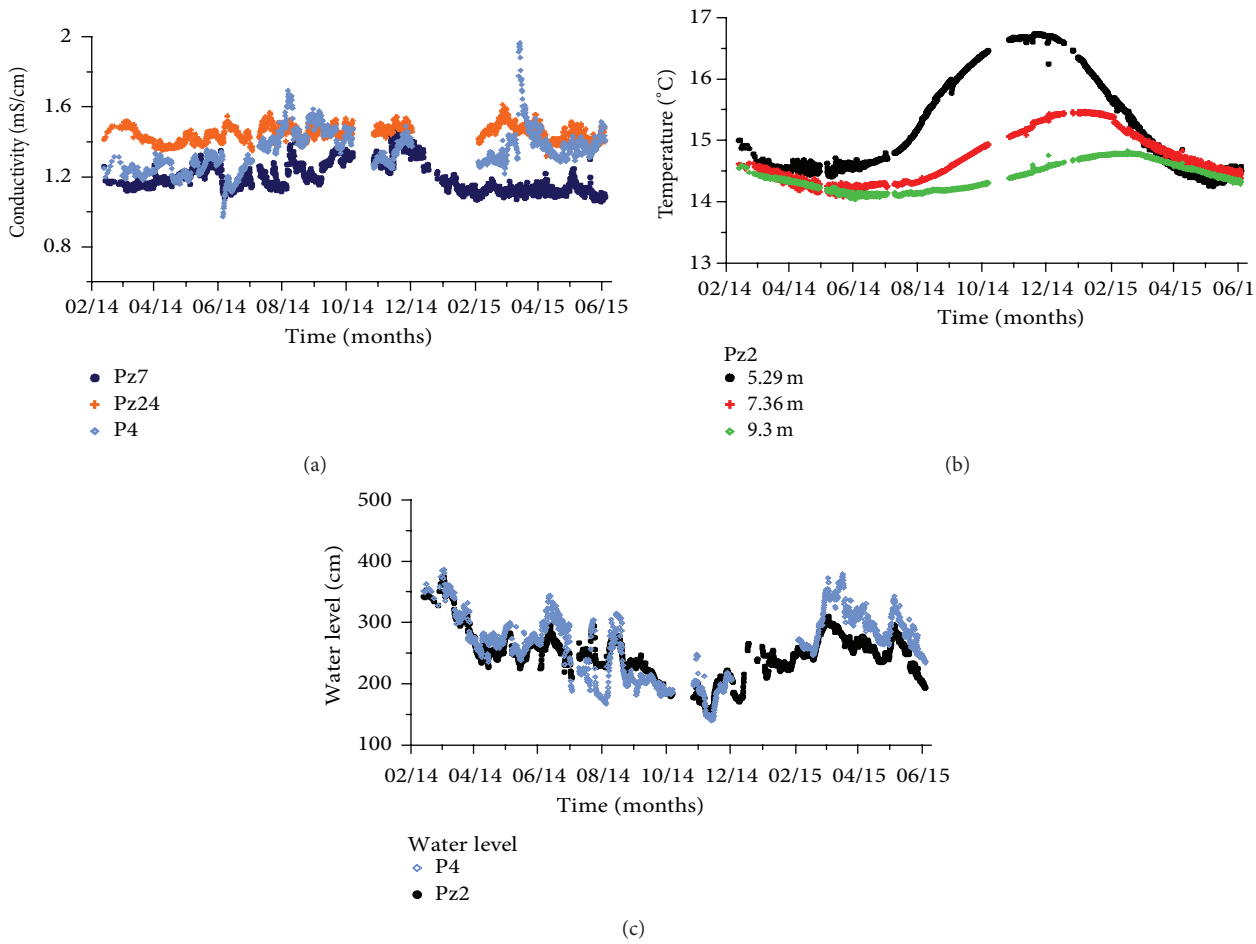

FIGURE 9: Water conductivity (a) and temperature (b) and ground water level (c) evolution over time.

changes in fluxes are supposed to be only due to temperature and moisture conditions. The difference of flux with season at this point was subtracted from the values obtained at the other measuring points to keep only the flux variations due to bacterial activity (degradation of natural organic matter and hydrocarbons) (Table 2). A seasonal variation of the CO_2 emissions is still monitored (Figure 11): there were more emissions during summer and fall, when groundwater level is low (Figure 9(c)), water temperature is warmer (Figures 9(b) and 10(b)), and ground is less moist (Figure 10(c)).

Moreover, CO_2 emissions had been measured with an isotopic signature typical of hydrocarbon biodegradation. Indeed, $\delta^{13}C(CO_2)$ were measured between −27 and −30‰ versus VPDB since February 2014 (Figure 12(a)), in accordance with the BTEX $\delta^{13}C$ signature measured in water (around −25 to −26‰ versus VPDB) (Figure 12(b)). Besides, CO_2 released at the surface originates from a more or less degraded BTEX located below the gas measuring station. Indeed, in December 2014, average evolution of $\delta^{13}C$(benzene) increased from (−28.1 ± 0.5)‰ to (−26.7 ± 1.2)‰ and $\delta^{13}C$(toluene) increased from (−27.4 ± 0.4)‰ to (−24.8 ± 1.9)‰, from upstream to downstream the pollution plume. At the same time, $\delta^{13}C(CO_2)$ increased, from upstream to downstream as well, from (−30.5 ± 0.7)‰ to (−28.3 ± 1.6)‰ in July 2014 and from (−28.1 ± 1.1)‰ to (−27.0 ± 1.2)‰ in October 2014 [49]. Although these $\delta^{13}C(CO_2)$ values were only a few per mil less than the $\delta^{13}(CO_2)$ from microbial degradation of plant material, $\delta^{13}(CO_2)$ showed a light isotopic fractionation (1 to 3‰) through the stream of the pollution plume:

(i) $\delta^{13}(CO_2)$ was lower than $\delta^{13}C$(hydrocarbon source).

(ii) The pollutant was enriched in ^{13}C when it was degraded, when residual BTEX concentrations were lower than 2000 $\mu g \cdot L^{-1}$.

(iii) The CO_2 tended to be depleted in ^{13}C, when fluxes were higher than 20 $\mu mol \cdot m^{-2} \cdot s^{-1}$.

It means that molecules with light isotopes (^{12}C) were preferred by bacterial metabolism. This is a typical isotopic fractionation due to biodegradation. This is in agreement with one example of a successful field application of isotopic assessment of biodegradation in an aviation gasoline contaminated aquifer where aerobic biodegradation of the gasoline constituents produced significantly enriched CO_2 [54]: the $\delta^{13}C(CO_2)$ values were ranging from −22.0 to −26.3‰, soil organic matter for the site ranged from −13.5 to −26.1‰, and the aviation gasoline $\delta^{13}C$ values were between

Table 2: Corrections made to CO_2 measurements from April 2014 to April 2015 (February 2014 is the baseline, uncorrected) from gas measuring point number 7.

	Apr. 2014	May 2014	June 2014	July 2014	Aug. 2014	Oct. 2014	Dec. 2014	Feb. 2015	Apr. 2015
Corrections (μmol·m^{-2}·s^{-1})	−0.6	−1.4	−3.05	−7.87	−9.9	−7.65	+1.22	+1.2	−3.27

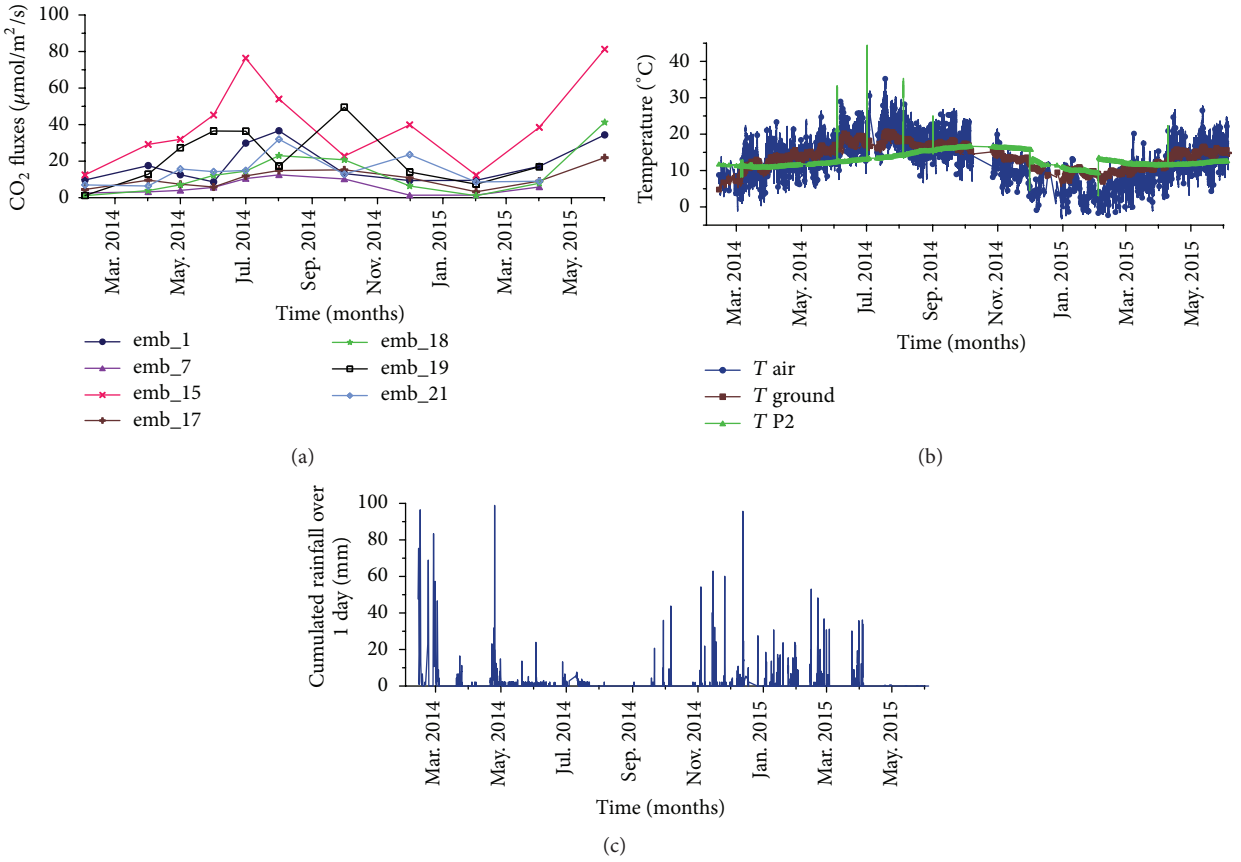

Figure 10: Measured CO_2 emissions (a); air, ground, and water temperatures (b); and rainfall (c) over time.

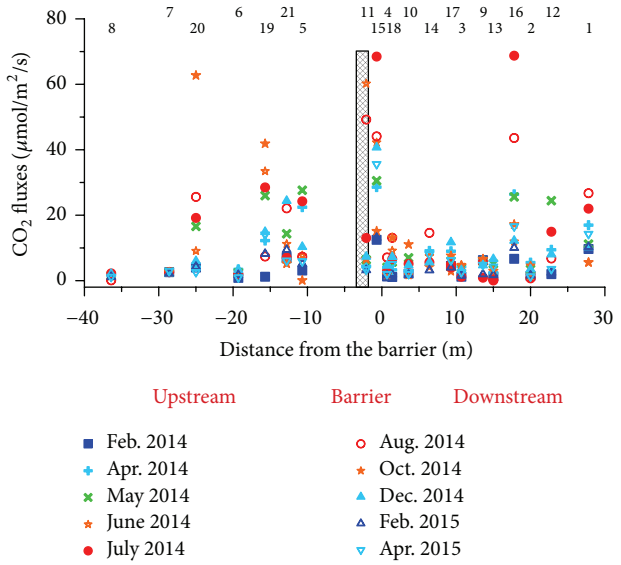

Figure 11: Measured CO_2 emissions (corrected from meteorological conditions) as a function of gas metering station location, for one year of monitoring.

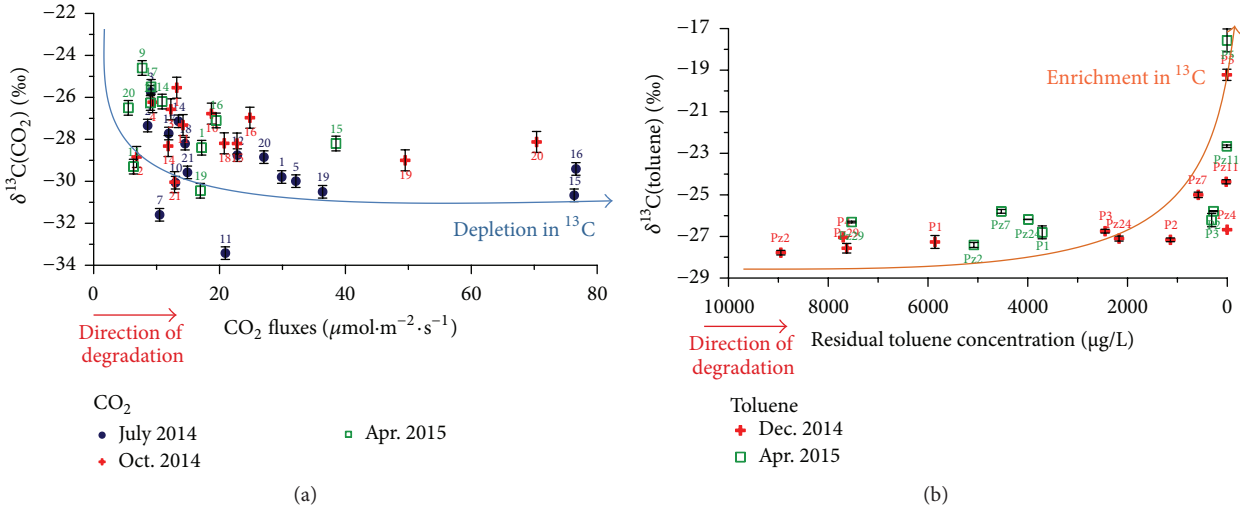

FIGURE 12: Carbon isotopic ratio versus VPDB of CO_2 (a) in function of CO_2 fluxes at the ground surface and carbon isotopic ratio versus VPDB of residual toluene (b) as a function of toluene concentrations in water.

−20.5 and −27.3‰. Conrad et al. (1999) [54] concluded that the difference of $\delta^{13}C$ was discernible. Another study from Aelion et al. (1997) [55] was carried out at a gasoline contaminated groundwater site under aerobic degradation. Although some of the $\delta^{13}C(CO_2)$ values from the contaminated site (between −35.9 and −22.0‰) overlapped with background $\delta^{13}C(CO_2)$ (between −22.9 and −23.9‰) from uncontaminated areas, on average the stable isotopic values were distinguishable between the contaminated and background sites.

4. Integration of Results and Conclusion

At the pilot site, the combination of geoelectrical measurements (ER and TDIP) with CO_2 analyses (fluxes and carbon isotopic ratios) was tested as monitoring tools to follow an enhanced biodegradation of hydrocarbons.

The results from the baseline characterisation in February-March 2014 had shown a more conductive and chargeable zone, around 3 meters in depth, which matches the polluted zone defined by geochemical borehole analyses, at the top of the water table (Figures 1, 3, 4, and 13). In this area, it can be assumed that there are numerous chargeable bacteria and production of conductive metabolites due to the pollutant degradation. This is consistent with the age of the gasoline leakage (almost twenty years ago), sufficient to allow the development of natural bacterial flora able to degrade hydrocarbons [56, 57] and to transform an electrical resistive substance in a more conductive one [12]. Moreover, CO_2 emissions were strong in this area and had an isotopic signature typical of hydrocarbon biodegradation. However, the overlap between $\delta^{13}C(CO_2)$ values from uncontaminated areas (plant root respiration and organic matter degradation) and from contaminated areas (with petroleum hydrocarbon degradation in addition) suggests that the combined measurement of $\delta^{13}C(CO_2)$ and $\delta^{13}C(BTEX)$ may be needed to confirm that the CO_2 is indeed from the contaminant degradation and not from microbial metabolism of natural plant materials. The northern zone of the site must be considered as a potential contaminated zone as well, accepting that the CO_2 emissions (measuring points 1, 12, and 16) are a sign of biodegradation and not the result of the presence of gas preferential pathways in this area (Figure 13).

The treatment for enhanced biodegradation was started in April 2014, with the activation of the reactive barrier that brought oxygen to the water table to stimulate aerobic biometabolism. The regular monitoring over one year showed that the area of biodegradation was still detected by both indirect methods (Figure 13). Moreover, a seasonal variation (after correction of effects associated with groundwater and soil temperature and soil moisture) for both electrical and gas monitoring was highlighted. Indeed, we observed highest conductivities of the ground at the end of summer and during fall, seasons when the piezometer probes measured the warmer groundwater temperatures (Figure 9(b)). The inverted resistivity sections were adjusted from temperature effect [52, 53], with a correction limited at groundwater level. In piezometer Pz2, at 5.29 m depth, the highest variation of temperature over a year is of the order of 2°C (Figure 9(b)), which corresponds to a variation of resistivity (1.4% per °C) lower than 3%. Nonetheless, a significant decrease in resistivity up to 15% was observed in the area of biodegradation at the end of the summer of 2014 and such a seasonal variation cannot be seen on water conductivity (Figure 9(a)). However, there is also a seasonal variation of the bacterial activity: when groundwaters are warmer, bacterial activity is more intensive and degrades more hydrocarbons and should produce more conductive metabolites [58–62]. Similarly, gas analyses, mainly CO_2 fluxes measurements, showed a seasonal variation. However, this should be mainly due to variation of soil respiration processes; otherwise we would have observed a seasonal variation in BTEX isotopic signatures. On the basis of this analysis, it is possible to make an assertion that seasonal variation of biodegradation processes was detected by our nonintrusive monitoring tools, especially by geoelectrical measurements.

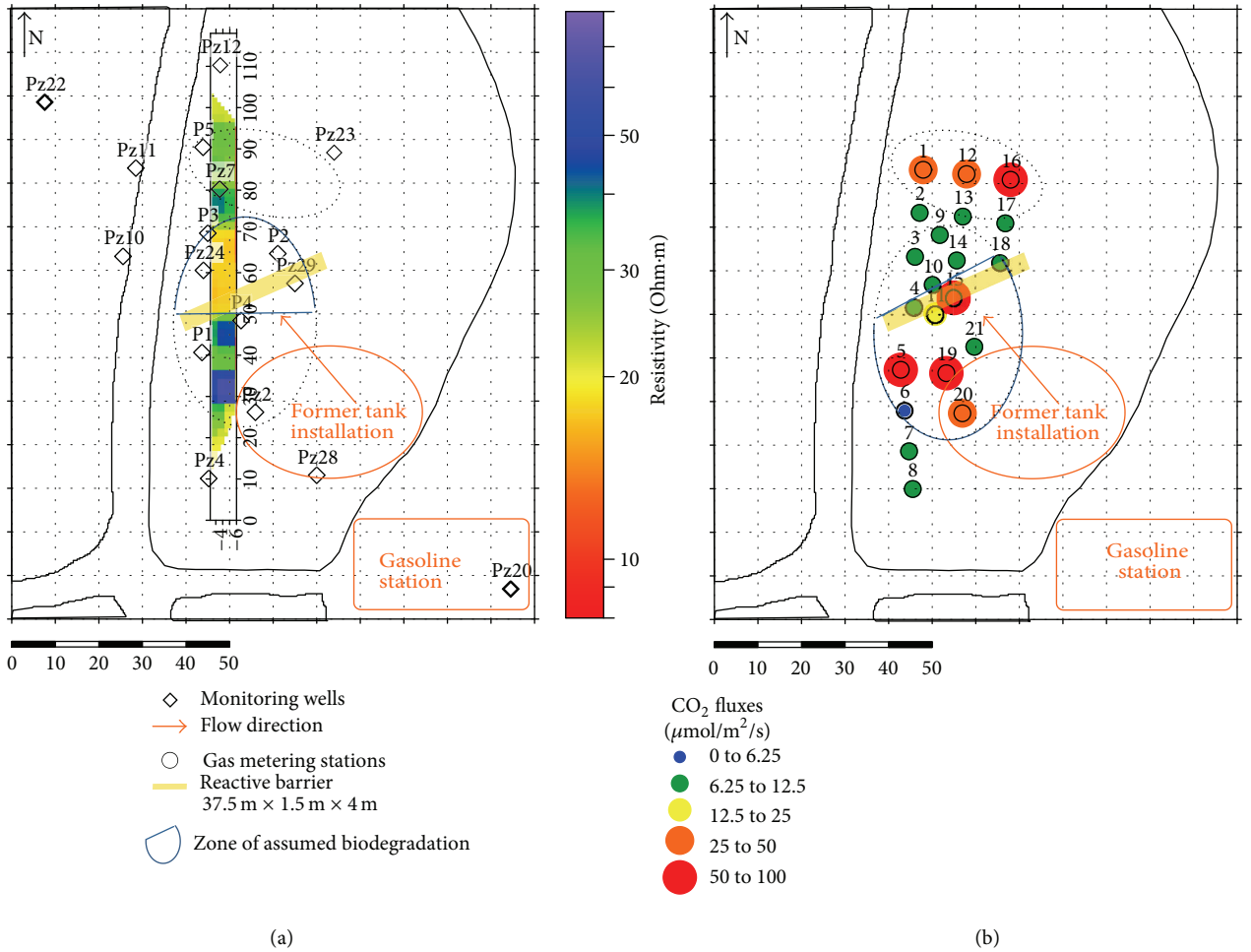

FIGURE 13: Maps of electrical resistivity measured on the permanent profile (a) and of measured CO_2 emissions (b), in July 2014. The elliptical shape highlights the area of biodegradation with production of conductive metabolites and CO_2.

However, the permeability of the ground is low and the groundwater table velocity is around 17 m/year. The oxygen from the barrier diffused slowly and its effect was not detected by both direct and indirect monitoring. The seasonal variation of bacterial activity was not yet "erased" by the continuous oxygen injection. Nonetheless, our first results over a year of monitoring show the interest of using geophysical methods and gas analyses to monitor and evaluate *in situ* remediation.

By applying the technology described here, fewer piezometers will be required for the monitoring and the understanding of bioremediation processes, leading to significant cost saving due to fewer monitoring requirements (piezometers, samples, and lab analyses) and more optimized remedial applications based on rapid identification of missed target zones.

Conflict of Interests

The authors declare that there is no conflict of interests regarding the publication of this paper.

Acknowledgments

The authors acknowledge the French Research Agency (Project BIOPHY, ANR-10-ECOT-014) and LABEX VOLTAIRE (Excellence Laboratory for Atmosphere, Resources and Environmental Interactions Study, University of Orleans, France) (ANR-10-LABX-100-01) for financial support. They also thank all the cooperation partners of the BIOPHY project: BRGM, LPC2E, Serpol, and Total. The LPC2E technical research team is gratefully acknowledged for their contribution to the development of the SPIRIT instrument. Technical support from BRGM is greatly appreciated as well. And they thank P. Gaudry, S. Williams, and G. Belot (LPC2E master's students) for their help during *in situ* measurement campaigns, as well as E. Verardo (BRGM Ph.D. student) for her contribution.

References

[1] N. Das and P. Chandran, "Microbial degradation of petroleum hydrocarbon contaminants: an overview," *Biotechnology Research International*, vol. 2011, Article ID 941810, 13 pages, 2011.

[2] F. Nadim, G. E. Hoag, S. Liu, R. J. Carley, and P. Zack, "Detection and remediation of soil and aquifer systems contaminated with petroleum products: an overview," *Journal of Petroleum Science and Engineering*, vol. 26, no. 1–4, pp. 169–178, 2000.

[3] K.-F. Chen, C.-M. Kao, C.-W. Chen, R. Y. Surampalli, and M.-S. Lee, "Control of petroleum-hydrocarbon contaminated groundwater by intrinsic and enhanced bioremediation," *Journal of Environmental Sciences*, vol. 22, no. 6, pp. 864–871, 2010.

[4] M. Farhadian, C. Vachelard, D. Duchez, and C. Larroche, "In situ bioremediation of monoaromatic pollutants in groundwater: a review," *Bioresource Technology*, vol. 99, no. 13, pp. 5296–5308, 2008.

[5] J. V. Weiss and I. M. Cozzarelli, "Biodegradation in contaminated aquifers: incorporating microbial/molecular methods," *Ground Water*, vol. 46, no. 2, pp. 305–322, 2008.

[6] M. Majone, R. Verdini, F. Aulenta et al., "In situ groundwater and sediment bioremediation: barriers and perspectives at European contaminated sites," *New Biotechnology*, vol. 32, no. 1, pp. 133–146, 2015.

[7] A. Flores Orozco, A. Kemna, C. Oberdörster et al., "Delineation of subsurface hydrocarbon contamination at a former hydrogenation plant using spectral induced polarization imaging," *Journal of Contaminant Hydrology*, vol. 136-137, pp. 131–144, 2012.

[8] J. A. Sogade, F. Scira-Scappuzzo, Y. Vichabian et al., "Induced-polarization detection and mapping of contaminant plumes," *Geophysics*, vol. 71, no. 3, pp. B75–B84, 2006.

[9] H. Vanhala, "Mapping oil-contaminated sand and till with the Spectral Induced Polarization (SIP) method," *Geophysical Prospecting*, vol. 45, no. 2, pp. 303–326, 1997.

[10] G. R. Olhoeft, "Direct detection of hydrocarbon and organic chemicals with ground penetrating radar and complex resistivity," in *Proceedings of the NWWA/API Conference on Petroleum Hydrocarbons and Organic Chemicals in Ground Water-Prevention, Detection and Restoration*, Houston, Tex, USA, November 1986.

[11] F. M. Mewafy, D. D. Werkema, E. A. Atekwana et al., "Evidence that bio-metallic mineral precipitation enhances the complex conductivity response at a hydrocarbon contaminated site," *Journal of Applied Geophysics*, vol. 98, pp. 113–123, 2013.

[12] E. A. Atekwana and E. A. Atekwana, "Geophysical signatures of microbial activity at hydrocarbon contaminated sites: a review," *Surveys in Geophysics*, vol. 31, no. 2, pp. 247–283, 2010.

[13] E. A. Atekwana and L. D. Slater, "Biogeophysics: a new frontier in Earth science research," *Reviews of Geophysics*, vol. 47, no. 4, Article ID RG4004, 2009.

[14] W. A. Sauck, "A model for the resistivity structure of LNAPL plumes and their environs in sandy sediments," *Journal of Applied Geophysics*, vol. 44, no. 2-3, pp. 151–165, 2000.

[15] V. Naudet and A. Revil, "A sandbox experiment to investigate bacteria-mediated redox processes on self-potential signals," *Geophysical Research Letters*, vol. 32, no. 11, Article ID L11405, 2005.

[16] N. Schwartz, T. Shalem, and A. Furman, "The effect of organic acid on the spectral-induced polarization response of soil," *Geophysical Journal International*, vol. 197, no. 1, pp. 269–276, 2014.

[17] R. Albrecht, J. C. Gourry, M.-O. Simonnot, and C. Leyval, "Complex conductivity response to microbial growth and biofilm formation on phenanthrene spiked medium," *Journal of Applied Geophysics*, vol. 75, no. 3, pp. 558–564, 2011.

[18] C. A. Davis, E. Atekwana, E. Atekwana, L. D. Slater, S. Rossbach, and M. R. Mormile, "Microbial growth and biofilm formation in geologic media is detected with complex conductivity measurements," *Geophysical Research Letters*, vol. 33, no. 18, Article ID L18403, 2006.

[19] A. Arato, M. Wehrer, B. Biró, and A. Godio, "Integration of geophysical, geochemical and microbiological data for a comprehensive small-scale characterizationof an aged LNAPL-contaminated site," *Environmental Science and Pollution Research*, vol. 21, no. 15, pp. 8948–8963, 2014.

[20] G. Cassiani, A. Binley, A. Kemna et al., "Noninvasive characterization of the Trecate (Italy) crude-oil contaminated site: links between contamination and geophysical signals," *Environmental Science and Pollution Research*, vol. 21, no. 15, pp. 8914–8931, 2014.

[21] R. M. Rosales, P. Martínez-Pagan, A. Faz, and J. Moreno-Cornejo, "Environmental monitoring using Electrical Resistivity Tomography (ERT) in the subsoil of three former petrol stations in SE of Spain," *Water, Air, and Soil Pollution*, vol. 223, no. 7, pp. 3757–3773, 2012.

[22] V. Che-Alota, E. A. Atekwana, E. A. Atekwana, W. A. Sauck, and D. D. Werkema Jr., "Temporal geophysical signatures from contaminant-mass remediation," *Geophysics*, vol. 74, no. 4, pp. B113–B123, 2009.

[23] K. H. Williams, A. Kemna, M. J. Wilkins et al., "Geophysical monitoring of coupled microbial and geochemical processes during stimulated subsurface bioremediation," *Environmental Science & Technology*, vol. 43, no. 17, pp. 6717–6723, 2009.

[24] K. Kaufmann, M. Christophersen, A. Buttler, H. Harms, and P. Höhener, "Microbial community response to petroleum hydrocarbon contamination in the unsaturated zone at the experimental field site Værløse, Denmark," *FEMS Microbiology Ecology*, vol. 48, no. 3, pp. 387–399, 2004.

[25] C. M. Aelion, P. Höhener, D. Hunkeler, and R. Aravena, *Environmental Isotopes in Biodegradation and Bioremediation*, CRC Press, Taylor & Francis, 2010.

[26] T. W. Boutton, "Stable carbon isotope ratios of natural materials: II. Atmospheric, terrestrial, marine, and freshwater environments," in *Carbon Isotope Techniques*, vol. 1, chapter 11, pp. 173–185, Academic Press, 1991.

[27] J. H. Troughton and K. A. Card, "Temperature effects on the carbon-isotope ratio of C3, C4 and crassulacean-acid-metabolism (CAM) plants," *Planta*, vol. 123, no. 2, pp. 185–190, 1975.

[28] C. Körner, G. D. Farquhar, and Z. Roksandic, "A global survey of carbon isotope discrimination in plants from high altitude," *Oecologia*, vol. 74, no. 4, pp. 623–632, 1988.

[29] R. U. Meckenstock, B. Morasch, C. Griebler, and H. H. Richnow, "Stable isotope fractionation analysis as a tool to monitor biodegradation in contaminated acquifers," *Journal of Contaminant Hydrology*, vol. 75, no. 3-4, pp. 215–255, 2004.

[30] S.-J. Kim, D. H. Choi, D. S. Sim, and Y.-S. Oh, "Evaluation of bioremediation effectiveness on crude oil-contaminated sand," *Chemosphere*, vol. 59, no. 6, pp. 845–852, 2005.

[31] O. Schoefs, M. Perrier, and R. Samson, "Estimation of contaminant depletion in unsaturated soils using a reduced-order biodegradation model and carbon dioxide measurement," *Applied Microbiology and Biotechnology*, vol. 64, no. 1, pp. 53–61, 2004.

[32] N. E.-D. Sharabi and R. Bartha, "Testing of some assumptions about biodegradability in soil as measured by carbon dioxide

evolution," *Applied and Environmental Microbiology*, vol. 59, no. 4, pp. 1201–1205, 1993.

[33] N. J. Sihota, O. Singurindy, and K. U. Mayer, "CO_2-Efflux measurements for evaluating source zone natural attenuation rates in a petroleum hydrocarbon contaminated aquifer," *Environmental Science and Technology*, vol. 45, no. 2, pp. 482–488, 2011.

[34] N. J. Sihota and K. U. Mayer, "Characterizing vadose zone hydrocarbon biodegradation using carbon dioxide effluxes, isotopes, and reactive transport modeling," *Vadose Zone Journal*, vol. 11, no. 4, 2012.

[35] P. K. Aggarwal, M. E. Fuller, M. M. Gurgas, J. F. Manning, and M. A. Dillon, "Use of stable oxygen and carbon isotope analyses for monitoring the pathways and rates of intrinsic and enhanced in situ biodegradation," *Environmental Science & Technology*, vol. 31, no. 2, pp. 590–596, 1997.

[36] M. E. Conrad, P. F. Daley, M. L. Fischer, B. B. Buchanan, T. Leighton, and M. Kashgarian, "Combined 14C and δ13C monitoring of in situ biodegradation of petroleum hydrocarbons," *Environmental Science and Technology*, vol. 31, no. 5, pp. 1463–1469, 1997.

[37] P. K. Aggarwal and R. E. Hinchee, "Monitoring in situ biodegradation of hydrocarbons by using stable carbon isotopes," *Environmental Science & Technology*, vol. 25, no. 6, pp. 1178–1180, 1991.

[38] K. H. Suchomel, D. K. Kreamer, and A. Long, "Production and transport of carbon dioxide in a contaminated vadose zone: a stable and radioactive carbon isotope study," *Environmental Science & Technology*, vol. 24, no. 12, pp. 1824–1831, 1990.

[39] C. Noel, J. C. Gourry, J. Deparis, I. Ignatiadis, F. Battaglia-Brunet, and C. Guimbaud, "Suitable real time monitoring of the aerobic biodegradation of toluene in contaminated sand by Spectral Induced Polarization measurements and CO_2 analyses," *Near Surface Geophysics*, In press.

[40] E. Verardo, A. Saada, V. Guerin et al., "Cas d'étude de gestion de site par atténuation naturelle: site 3—hydrocarbures pétroliers," Project ATTENA—Phase 2, Final Report, ADEME, 2013.

[41] R. Boopathy, "Factors limiting bioremediation technologies," *Bioresource Technology*, vol. 74, no. 1, pp. 63–67, 2000.

[42] R. M. Atlas, "Microbial hydrocarbon degradation—bioremediation of oil spills," *Journal of Chemical Technology & Biotechnology*, vol. 52, no. 2, pp. 149–156, 1991.

[43] L. D. Slater and D. Lesmes, "IP interpretation in environmental investigations," *Geophysics*, vol. 67, no. 1, pp. 77–88, 2002.

[44] M. H. Loke, J. E. Chambers, and R. D. Ogilvy, "Inversion of 2D spectral induced polarization imaging data," *Geophysical Prospecting*, vol. 54, no. 3, pp. 287–301, 2006.

[45] H. Craig, "Isotopic standards for carbon and oxygen and correction factors for mass-spectrometric analysis of carbon dioxide," *Geochimica et Cosmochimica Acta*, vol. 12, no. 1-2, pp. 133–149, 1957.

[46] C. Guimbaud, V. Catoire, S. Gogo et al., "A portable infrared laser spectrometer for field measurements of trace gases," *Measurement Science and Technology*, vol. 22, pp. 1–17, 2011.

[47] S. Gogo, C. Guimbaud, F. Laggoun-Défarge, V. Catoire, and C. Robert, "In situ quantification of CH4 bubbling events from a peat soil using a new infrared laser spectrometer," *Journal of Soils and Sediments*, vol. 11, no. 4, pp. 545–551, 2011.

[48] A. Grossel, B. Nicoullaud, H. Bourennane et al., "Simulating the spatial variability of nitrous oxide emission from cropped soils at the within-field scale using the NOE model," *Ecological Modelling*, vol. 288, pp. 155–165, 2014.

[49] C. Guimbaud, C. Noel, M. Chartier et al., "A quantum cascade laser infrared spectrometer for CO_2 stable isotope analysis: field implementation at a hydrocarbon contaminated site under bioremediation," *Journal of Environmental Sciences*, 2016.

[50] J. W. Raich and A. Tufekcioglu, "Vegetation and soil respiration: correlations and controls," *Biogeochemistry*, vol. 48, no. 1, pp. 71–90, 2000.

[51] J. W. Raich and C. S. Potter, "Global patterns of carbon dioxide emissions from soils," *Global Biogeochemical Cycles*, vol. 9, no. 1, pp. 23–36, 1995.

[52] K. Hayley, L. R. Bentley, M. Gharibi, and M. Nightingale, "Low temperature dependence of electrical resistivity: implications for near surface geophysical monitoring," *Geophysical Research Letters*, vol. 34, no. 18, 2007.

[53] M. Hayashi, "Temperature-electrical conductivity relation of water for environmental monitoring and geophysical data inversion," *Environmental Monitoring and Assessment*, vol. 96, no. 1–3, pp. 119–128, 2004.

[54] M. E. Conrad, A. S. Templeton, P. F. Daley, and L. Alvarez-Cohen, "Isotopic evidence for biological controls on migration of petroleum hydrocarbons," *Organic Geochemistry*, vol. 30, no. 8, pp. 843–859, 1999.

[55] C. M. Aelion, B. C. Kirtland, and P. A. Stone, "Radiocarbon assessment of aerobic petroleum bioremediation in the vadose zone and groundwater at an AS/SVE site," *Environmental Science & Technology*, vol. 31, no. 12, pp. 3363–3370, 1997.

[56] C.-H. Chaîneau, J.-L. Morel, and J. Oudot, "Microbial degradation in soil microcosms of fuel oil hydrocarbons from drilling cuttings," *Environmental Science & Technology*, vol. 29, no. 6, pp. 1615–1621, 1995.

[57] J. R. Van der Meer, W. M. de Vos, S. Harayama, and A. J. B. Zehnder, "Molecular mechanisms of genetic adaptation to xenobiotic compounds," *Microbiological Reviews*, vol. 56, no. 4, pp. 677–694, 1992.

[58] J. G. Leahy and R. R. Colwell, "Microbial degradation of hydrocarbons in the environment," *Microbiological Reviews*, vol. 54, no. 3, pp. 305–315, 1990.

[59] F. Garnier, *Contribution à L'évaluation Biogéochimique des Impacts Liés à L'exploitation Géothermique des Aquifères Superficiels: Expérimentations et Simulations à L'échelle D'un Pilote et D'installations Réelles*, Université d'orléans, 2012.

[60] M. Lenczewski, P. Jardine, L. McKay, and A. Layton, "Natural attenuation of trichloroethylene in fractured shale bedrock," *Journal of Contaminant Hydrology*, vol. 64, no. 3-4, pp. 151–168, 2003.

[61] B. A. Bekins, I. M. Cozzarelli, E. M. Godsy, E. Warren, H. I. Essaid, and M. E. Tuccillo, "Progression of natural attenuation processes at a crude oil spill site: II. Controls on spatial distribution of microbial populations," *Journal of Contaminant Hydrology*, vol. 53, no. 3-4, pp. 387–406, 2001.

[62] G. Lu, T. P. Clement, C. Zheng, and T. H. Wiedemeier, "Natural attenuation of BTEX compounds: model development and field-scale application," *Ground Water*, vol. 37, no. 5, pp. 707–717, 1999.